Liquid Crystals
Publication details, including instructions for authors and subscription information:
http://www.informaworld.com/smpp/title~content=t713926090

Electric field effects on director pattern and disclinations in free standing nematic films of 8CB

K. S. Krishnamurthy; R. Balakrishnan

Online publication date: 11 November 2010

To cite this Article Krishnamurthy, K. S. and Balakrishnan, R.(2002) 'Electric field effects on director pattern and disclinations in free standing nematic films of 8CB', Liquid Crystals, 29: 3, 383 — 389
To link to this Article: DOI: 10.1080/02678290110101903
URL: http://dx.doi.org/10.1080/02678290110101903

LIQUID CRYSTALS, 2002, VOL. 29, NO. 3, 383–389

Electric field effects on director pattern and disclinations in free standing nematic films of 8CB

K. S. KRISHNAMURTHY* and R. BALAKRISHNAN

Applied Science Department, Faculty of Electrical and Mechanical Engineering, College of Military Engineering, Pune 411 031, India

(*Received 17 March 2001; in final form 27 August 2001; accepted 5 September 2001*)

Studies of electric field-induced orientational effects are carried out on substrate-free nematic 8CB films, held between parallel electrodes and containing a peripheral −1/2 loop. The loop separates the birefringent boundary from the central homeotropic zone. Static and dynamic characteristics of the splay–bend layers contiguous to the electrodes are investigated by polarizing microscopy. A model based on director field symmetry is proposed to explain (a) the growth of the transition layers independently of the associated singularities and (b) the formation or otherwise of static solitons (Brochard–Leger walls). Linear dependence of the growth rate of transition layers on field strength is compared with a similar behaviour for line defects. Bifurcation of a soliton at elevated voltages into a pair of −1/2 lines, through a non-pincement process, is described.

1. Introduction

Previous reports on electric field effects in substrate-free nematic films deal exclusively with electroconvective instabilities [1–4]. Purely orientational phenomena in freestanding nematics with well defined boundary conditions have up to now attracted little attention. It is the purpose of this study to characterize the field-induced orientational instabilities in a freely suspended nematic film of 8CB, with homeotropic anchoring at *all* the limiting surfaces. In this 'boundary normal' configuration, the central pseudo-isotropic zone is surrounded by a splay–bend transition layer next to the supporting edges. We discuss the static and dynamic features of the transition layers, formation of static solitons and transformation of solitons into disclinations.

2. Experimental

The 8CB sample was from BDH Chemicals, UK (K24) and exhibits the nematic phase from 33.5 to 41°C, between SmA and isotropic phases. The experimental geometry is shown in figure 1. The observations were made in transmitted mercury green light, under a Leica polarizing microscope equipped with a hot stage and a colour video camera (Sony CCD IRIS). The images were analysed using the Leica Q500 MC software. The results presented in this paper are for samples of thickness $d \sim 75\,\mu m$. Thin films ($d \sim 20\,\mu m$) display a markedly different behaviour associated with electroconvection and will be discussed elsewhere.

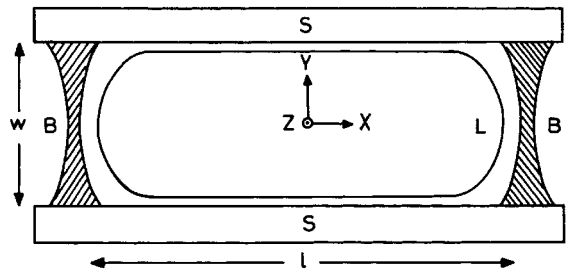

Figure 1. Top view of the film geometry showing the electrodes S, adhesive bridges B, disclination loop L, and reference axes (x, y, z). Observation along z; film thickness $d \sim 75\,\mu m$, length $\sim 15\,mm$, width $w = 470–525\,\mu m$.

3. Results and discussion

3.1. *Field variation of transition zone width*

The nematic films, even in the absence of any treatment to the supporting edges, show a spontaneous orientation of the molecules. Between crossed polarizers set diagonally with respect to the x and y directions, the sample texture consists of a series of parallel birefringence bands next to the electrode edges and on either side of the central dark zone, figure 2(*a*). The fringes are due to the transition layers that involve splay–bend deformations as ascertained using a tilting compensator.

* Author for correspondence; e-mail: gogosairam@vsnl.net

Liquid Crystals ISSN 0267-8292 print/ISSN 1366-5855 online © 2002 Taylor & Francis Ltd
http://www.tandf.co.uk/journals
DOI: 10.1080/02678290110101903

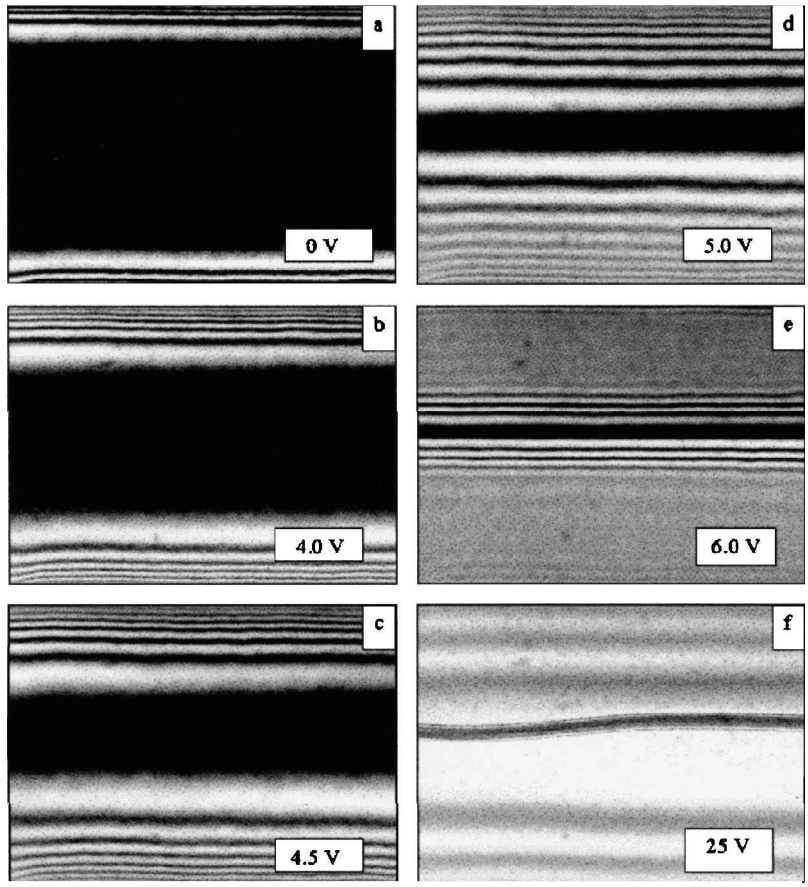

Figure 2. Birefringence fringes observed in 8CB at various indicated voltages in the region of transition layers; 100 Hz, 40°C, $w = 525$ μm.

Quite evidently a $-1/2$ disclination loop encloses the central homeotropic zone. The curved ends of the loop are clearly visible in the field free state, but the straight portions along x are pinned to the electrode edges and become visible only under high applied electric fields as will be discussed later.

Upon application of a gradually increasing field, the transition layers next to the electrode edges progressively widen (figure 2). The voltage variation of layer width, determined from the intensity profiles, is non-linear and nearly exponential (figure 3). The plot for lower frequency in figure 3 shows a more rapid variation beyond about 100 μm compared with that for 30 kHz. This may be attributed to the nature of the electric field lines for the two frequency regimes. For frequencies much larger than the charge relaxation frequency $\nu_c = 1/2\pi\rho\varepsilon$, where ρ and ε denote the appropriate electrical resistivity and dielectric constant respectively, the fluid acts as a non-conducting dielectric. This results in the field within the sample becoming non-uniform, being minimum at the centre of the sample and maximum near the electrode

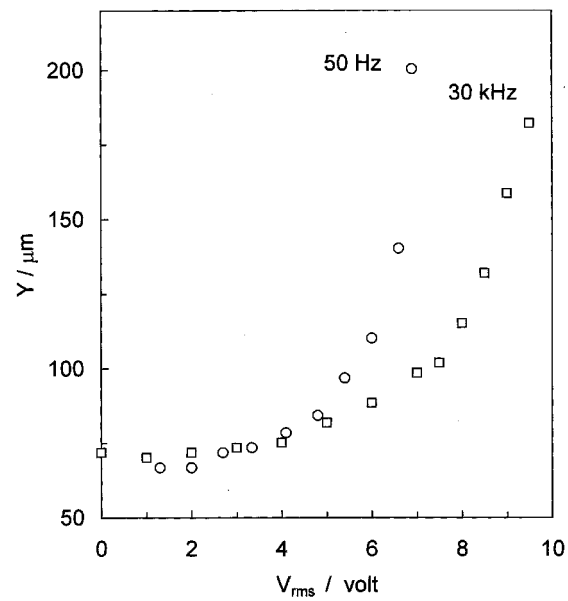

Figure 3. Voltage dependence of transition zone width in 8CB; $w = 470$ μm, 37°C.

edges. For low frequencies, this nonuniformity is absent and the field lines are as for a static field [2]. The value of v_c obtained from ρ and ε perpendicular to the director is $\sim$10 Hz for the samples studied.

3.2. *Director field*

The growth of the transition layers with increasing electric field is only to be expected from energy considerations in a nematic with positive dielectric anisotropy, such as 8CB ($\Delta\varepsilon \sim 7.5$, at 38°C). It is important to note, however, that a concomitant movement of the associated disclinations does not accompany this growth. In order to explain this and other results, we consider three possible director patterns differing in their mirror planes, σ. The pattern in figure 4 (*a*) has both σ_{xy} and σ_{xz}; that in figure 4 (*b*) has only σ_{xz}; and the one in figure 4 (*c*) has neither. Observation of the growth of transition layers in the absence of movement of disclinations excludes the possibility of the initial director pattern shown in figure 4 (*a*). Otherwise, assuming the symmetry of the original director pattern is undisturbed by the field, the on-state distortion should conform to either of the structures in figure 5. The configuration in figure 5 (*a*) is ruled out since no new defect lines are observed in the expanded transition layer regions. That in figure 5 (*b*), though in agreement with various experimental results, is considered improbable from the viewpoint of elastic energy since it restricts the midregion to remain homeotropic, while requiring the maximum reorientation to occur closer to the free surfaces.

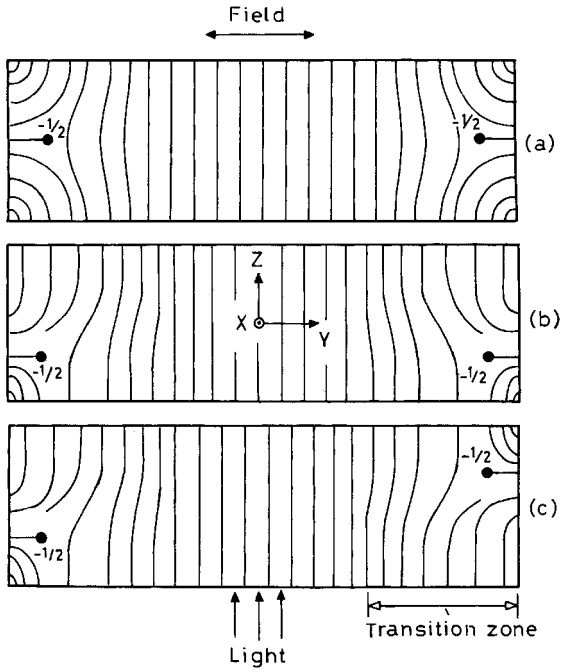

Figure 4. Three types of director configuration in the field free state. In (*a*) the disclinations at both the electrodes lie in the mid *xy* plane; in (*b*) the lines are below the midplane and, in (*c*) the lines are on either side of the midplane.

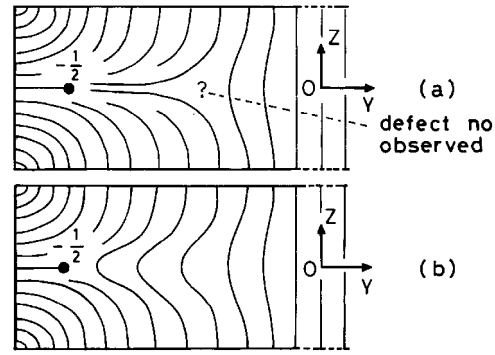

Figure 5. Hypothetical director configurations in the field-on state corresponding to an initial pattern as in figure 4 (*a*).

3.3. *Wall formation*

The birefringence fringes next to the electrode edges are generally not continuous, but appear in different segments; the fringes in a segment come into focus, broadly, in one of the two planes, depending on whether the associated disclination lies above or below the midplane. For instance, in figures 6 (*a–d*), showing the same sample region, there are three fringe segments at each of the electrodes; in (*a*) the central segments are in focus while the outer ones are blurred; in (*b*) it is the reverse. The transition layers growing with the field will, eventually, either form the Brochard–Leger (BL) wall or completely merge. For wall formation, the director field must be as in figure 4 (*b*) with the defect lines of the opposite layers located both below or above the mid *xy* plane. If the lines are situated as in figure 4 (*c*), no wall formation occurs since the director tilts are of same sign for the opposite layers. For all the three pairs of opposite segments in figure 6 (*a*), the condition for wall formation is fulfilled. However, the overall splay bend structure for the central pair is inverted with respect to that for the outer pairs. Thus, at higher fields, one common wall is formed along *x* in the midregion. It is flanked by two others in the central region, figures 6 (*c*, *d*). In figure 6 (*e*), the fringes at the top belong to a common segment and those at the bottom appear in three segments. Evidently, in the central region, where the director field is as in figure 4 (*c*), the transition layers merge without forming a wall at elevated voltages. However, in the outer regions, where the structure is as in figure 4 (*b*), walls form, figures 6 (*e*, *h*). The zigzag line in the lower part of figure 6 (*h*) is the disclination detached from the electrode edge.

It may be added that in thin films ($d \sim 20\,\mu$m) the disclination moves with the associated transition layer

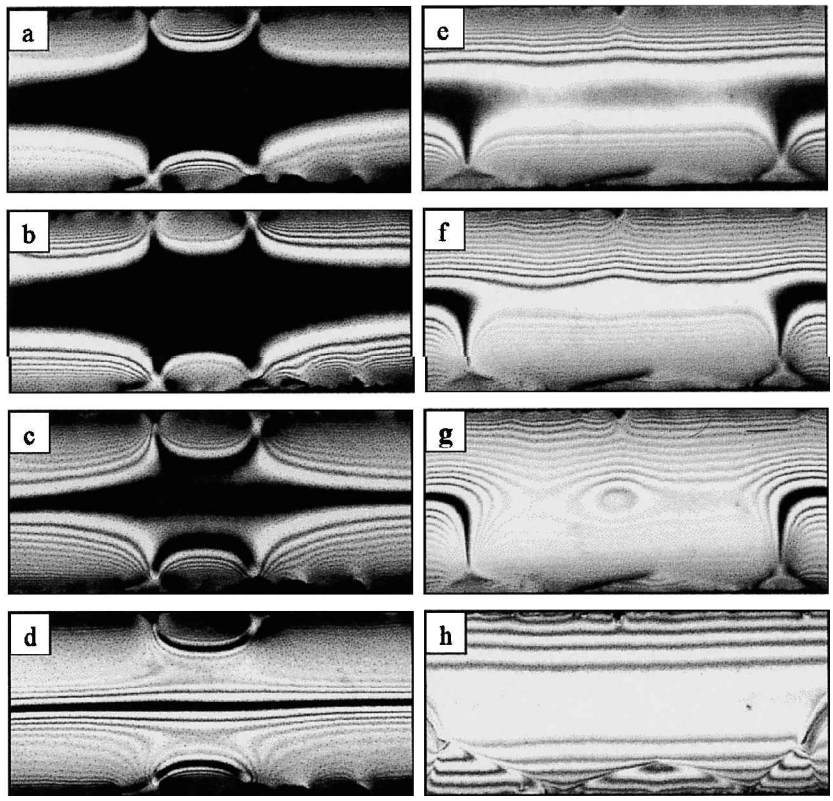

Figure 6. Textures to show two types of curvature of the splay–bend director distortion and their relevance to wall formation (see text). Figures (*a–d*) belong to one region, and (*e–f*) to another; $T = 36°C$. Voltages: 6, 6, 6.1 and 6.5 V for (*a–d*); 5.4, 6.4, 6.4 and 12.6 V for (*e–h*), respectively. Frequencies: 100 Hz for (*a–d*); 10 kHz for (*e–h*). For (*a*) and (*b*), the focal planes are different. Figures (*f*) and (*g*) were recorded at a few seconds interval under identical conditions.

and always remains at the layer-front in the field-on state. Therefore, the field in figure 4 (*a*) is appropriate for thin films.

3.4. *Wall characterization*

At what stage in their growth do the transition layers approaching each other form the BL wall? To answer this question, we may consider the layer width, measured in terms of the separation τ between the first two maxima of the corresponding birefringence pattern, as a function of voltage. This is shown in figure 7 and a transition is evident at ~ 7.8 V. For lower voltages, the layers apparently expand independently of each other, but above the threshold V_c, they merge to form a wall. The wall thickness δ, of which τ is now a measure [5, 6], conforms to the characteristics of the BL wall. For instance, according to the theoretical prediction of Brochard [7], wall thickness should diverge with decreasing field so that τ^{-2} varies as $(V^2 - V_c^2)$. More recently, Wang, from his theoretical analysis of the soliton properties of the BL wall, has predicted τ^{-2} to vary as $(V^3 - V^2 V_c)$ [8]. Figure 8 presents the $\tau - V$ dependence according to the two theories and, within the experimental accuracy, agreement with the results is equally good in both cases.

For a BL wall, it is also expected [7] that the mean tilt angle θ_m of the molecules should vary with the distance y from the core of the wall as

$$\theta_m = \theta_\infty \tanh\left(\frac{\theta_\infty y}{2\xi}\right)$$

Where θ_∞ and ξ denote the mean molecular tilt angle far from the wall and the coherence length, respectively. ξ/θ_∞ denotes the coherence length in the plane of the layer. We used the birefringence fringes to verify this equation. It may be seen that under the small angle approximation, θ_m^2 changes by a constant quantity between fringes. Thus by assuming the validity of the above equation at any three fringe locations, one can deduce $2\xi/\theta_\infty$ and then use it to construct the theoretical plot of $(\theta_m/\theta_\infty)^2$ as a function of y. Experimental fringe positions are found to be in agreement with this theoretical plot (figure 9).

3.5. *Transformation of wall into disclinations*

When a BL wall is sufficiently narrowed by the field to render it energetically unstable, it is expected to undergo bifurcation into a pair of disclinations of opposite sign.

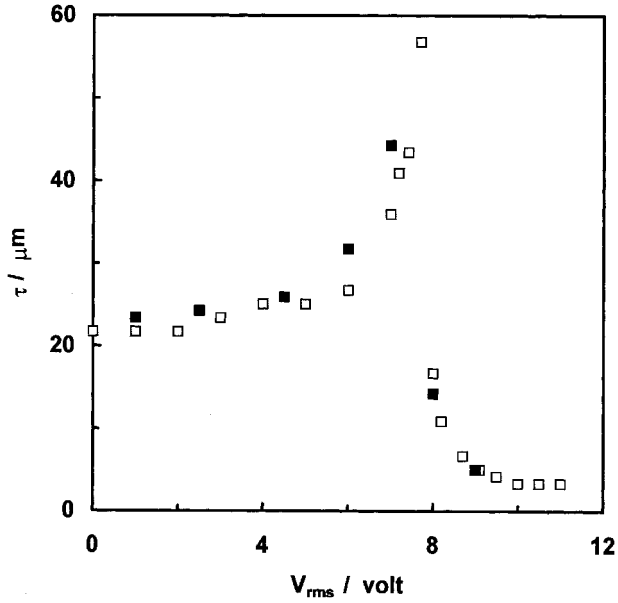

Figure 7. Voltage variation of the separation between first and second maxima in the birefringence fringe pattern observed in the transition layer region. BL wall forms at about 7.8 V: 30 Hz, 36°C, $w = 525\,\mu m$. Open and filled squares are, respectively, for increasing and decreasing voltage.

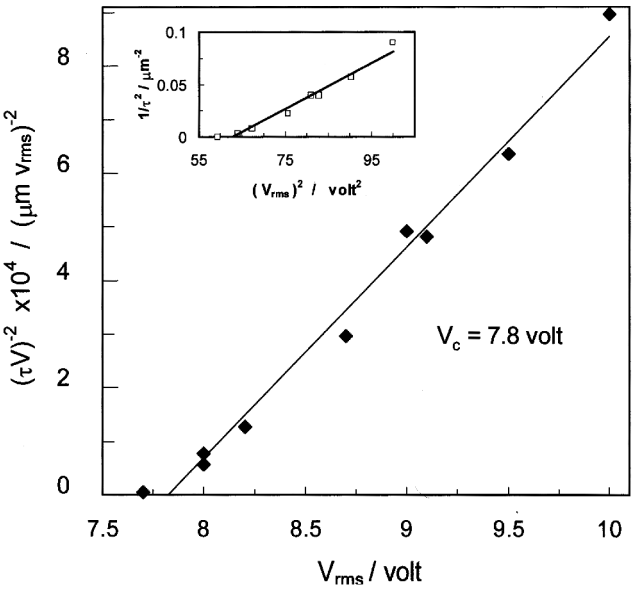

Figure 8. Dependence of wall thickness (measured in terms of τ, the distance between first two maxima) on voltage V according to [7]. The inset shows the dependence according to [8].

This is the well known pincement [9]. We do observe the decay and disappearance of walls to commence when the voltage reaches $\sim 2V_c$, but instead of pincement, an invasion of the initial disclination into the wall is observed. It is to be noted that the walls almost always

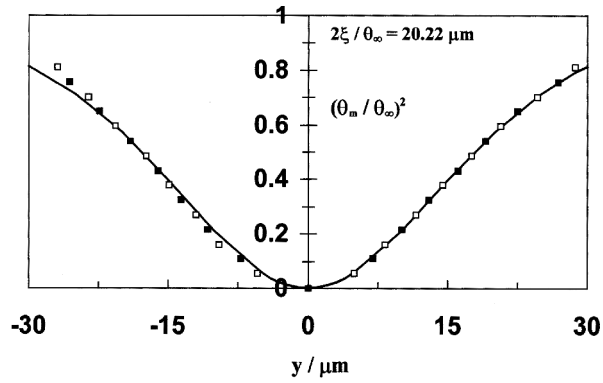

Figure 9. Dependence of the square of mean molecular tilt on the distance y from the centre of the splay–bend wall in 8CB; 37°C, 12 V, 13 kHz. Data are from an interferogram. Filled squares represent minima and open ones, maxima. In constructing the theoretical curve, locations of three fringes were assumed to obey the tanh law.

end on, and remain in equilibrium with segments of initial disclination line detached from the edges as in figures 6(*e–h*). At higher fields, these segments grow at the expense of the wall and, in so doing, appear to split into two lines each. In figures 10(*a–e*) illustrating this process, the black band is the wall. It is being encroached upon, at both ends, by segments of the line attached to the top edge. The thick bright lines and the fine dark ones are the $-1/2$ disclinations coming into focus at different levels. With time, bright lines form a loop with the line detaching from the top edge, shrink, and finally vanish, figures 10(*a–e*). In figure 10(*f*), showing four disclination lines, the one at the top is the initial line detaching from the edge and the two others below are replacements for a wall. The small initial line segment at the bottom will eventually become part of a vanishing loop. At a high voltage (~ 100 V), only two disclinations survive as a topological necessity. These are zigzag lines at higher frequencies, and located in the mid region. The zigzag nature may be attributed to elastic anisotropy [10]. The two lines which constantly drift side ways, appear sometimes in phase, figure 10(*g*), and sometimes out of phase, figure 10(*h*). If the frequency is lowered, the lines flex into various irregular shapes due to electrohydrodynamic effects, figure 10(*i*).

The invasion of the wall by the lines displays a definite threshold and occurs at a rate linear in voltage (figure 11). A similar behaviour has been reported by Stieb *et al.* [11] for a mixture of phenyl benzoates examined in the sandwich cell geometry.

3.6. *Dynamics of transition layers*

As described in § 3.1, upon application of a suitable electric field along y, the transition layers facing each other begin to expand into the central pseudoisotropic

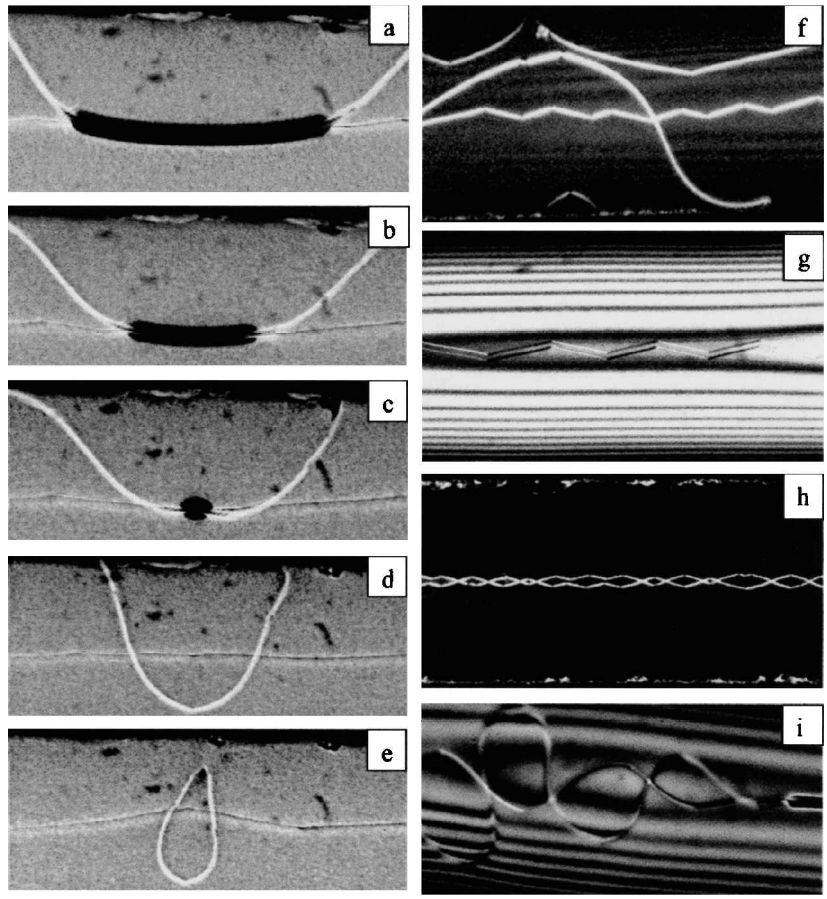

Figure 10. Time photographs in ordinary light at 14.4 V, 10 kHz, and 40°C (*a–e*). Disclinations under different conditions (*f–i*). 15.2 V, 1 kHz, 37°C, polarizers along *x* and *y* (*f*); 108 V, 13 kHz, 34.5°C, partially crossed polarizers (*g*); 25 V, 10 kHz, 37°C, polarizers along *x* and *y* (*h*); 16 V, 50 Hz, 37°C, crossed polarizers in diagonal position (*i*).

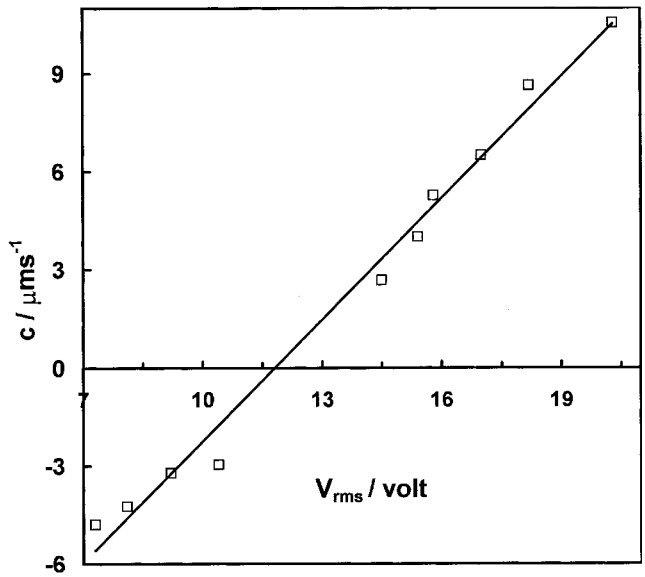

Figure 11. The speed *c* of transformation of wall into lines at various voltages in 8CB, 37°C, $w = 470\,\mu m$. Positive rate applies for bifurcation from wall to a pair of disclinations, and negative rate for the reverse process.

zone. The rate of this growth at a given field strength is determined by timing the passage of the first birefringence maximum through a distance of 100 μm after a sudden application of the field. This growth rate exhibits a linear response to the applied field of a given frequency. From the data in figure 12, the voltage variation of the growth rate is found to be $1.4\,\mu m\,V^{-1}\,s^{-1}$ at 100 Hz and $0.85\,\mu m\,V^{-1}\,s^{-1}$ at 30 kHz. The frequency dependence of growth rate is only to be expected from the variation of field configuration with frequency as mentioned in § 3.1.

It is relevant to recall here the electric field experiments of Cladis *et al.* [12] on the dynamics of $-1/2$ line defects in 5CB. They used a sample bound between glass substrates and electrode wires, and aligned in the boundary normal configuration; the $-1/2$ line defects, are first driven to the mid-region by a field along *y*; then this field is switched off and a vertical field along *z* is applied. Under these conditions the defect lines are found to translate toward electrodes with a speed proportional to the voltage. This behaviour is explained by considering the excess free energy per unit line-length,

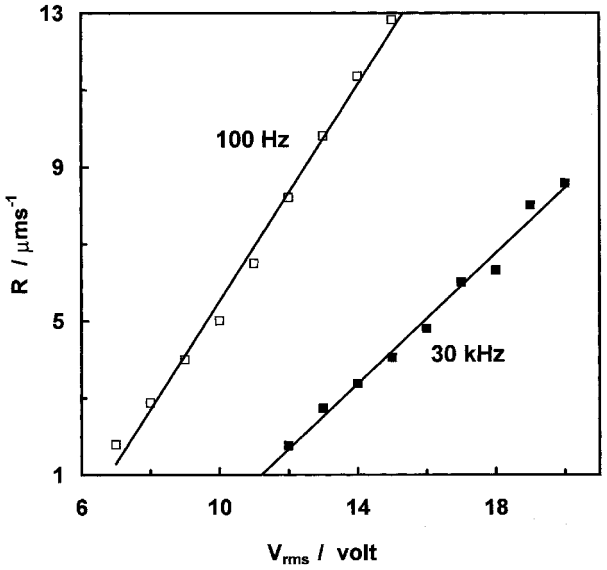

Figure 12. Growth rate R of transition zone as a function of applied voltage, $w = 470\ \mu m$, 37°C.

F_{exc}, of the distorted configuration over the homeotropic configuration, given by

$$F_{exc} = F_{core} + 2l(\Delta\varepsilon K)^{1/2} E$$

where l is the distance from the electrode to the defect line, $\Delta\varepsilon$ the absolute dielectric anisotropy, K the effective elastic constant, E the applied field, and F_{core} the free energy of the core region within a distance of the coherence length. From the distance independent force $-dF_{exc}/dl$, the velocity may be obtained as a linear function of E, the proportionality factor involving effective viscosity, K, $\Delta\varepsilon$ and a numerical constant. The experimental translational speed for 5CB varies as $4.7\ \mu m\ V^{-1}\ s^{-1}$, in agreement with the predicted value.

In our experiments, significantly, there is no motion of the defect line associated with the change in boundary layer thickness, which here is brought about only by the director rotation. However, we can apply the theory of Cladis *et al.* [12] to the present case since the core energy term does not enter the expression for force. We could visualize the force as acting on the boundary layer as whole, rather than the defect line. The effective viscosity term would then have to be suitably modified to take the rotational motion of the director into account.

4. Concluding remarks

It is clearly demonstrated that a half disclination attached to boundary walls does not respond to ordinary fields at which the director pattern associated with it readily propagates to lower the free energy. The speed of this propagation is linear in field, indicating that a distance independent electrical force governs it, just as in the case of disinclination lines free from boundary effects. It is further shown that a boundary layer, which by itself is not a BL type wall, may combine with another layer to produce the wall at a well marked threshold. It is possible to predict optically the formation or non-formation of walls based on the overall symmetry of director distribution. Finally, a pair of half-strength disclinations replaces the wall under a high field, in a non-pincement process that is reversible.

The authors wish to thank Professor N. V. Madhusudana and Dr P. E. Cladis for helpful suggestions; Professor Satyendra Kumar for the sample; and the Commandant, College of Military Engineering for experimental facilities and encouragement.

References

[1] Meyerhofer, D., Sussman, A., and Williams, R., 1972, *J. appl. Phys.*, **43,** 3685.
[2] Faetti, S., Fronzoni, L., and Rolla, P. A., 1983 *J. chem. Phys.*, **79,** 1427 and 5054.
[3] Morris, S. W., de Bruyn, J. R., and May, A. D., 1990, *Phys. Rev. Lett.*, **65,** 2378; Morris, S. W., de Bruyn, J. R., and May, A. D., 1991, *Phys. Rev. A*, **44,** 8146.
[4] Krishnamurthy, K. S., and Balakrishnan, R., 1997, *Mol. Cryst. liq. Cryst.*, **303,** 349.
[5] Krishnamurthy, K. S., and Bhate, M. S., 1985, *Mol. Cryst. liq. Cryst.*, **128,** 29.
[6] Leger, L., 1973, *Mol. Cryst. liq. Cryst.*, **24,** 33.
[7] Brochard, F., 1972, *J. Phys.*, **33,** 607.
[8] Wang, X. Y., 1985, *Phys. Lett.*, **112A,** 402.
[9] De Gennes, P. G., and Prost, J., 1993, *The Physics of Liquid Crystals*, 2nd Edn (New York: Oxford University Press), p. 190.
[10] Galerne, Y., Itoua, J., and Liebert, L., 1988, *J. Physique*, **49,** 681.
[11] Stieb, A., Baur, G., and Meier, G., 1975, *J. Physique*, **36,** C1-185.
[12] Cladis, P. E., van Saarloos, W., Finn, P. L., and Kortan, A. R., 1987, *Phys. Rev. Lett.*, **58,** 222.